Results in Physics 6 (2016) 704–711

Contents lists available at ScienceDirect

Results in Physics

journal homepage: www.journals.elsevier.com/results-in-physics

Secondary bending effects in progressively damaged single-lap, single-bolt composite joints

Libin Zhao [a], An Xin [a], Fengrui Liu [a], Jianyu Zhang [b,*], Ning Hu [b]

[a] School of Astronautics, Beihang University, Beijing 100191, China
[b] College of Aerospace Engineering, Chongqing University, Chongqing 400044, China

ARTICLE INFO

Article history:
Received 5 July 2016
Accepted 28 August 2016
Available online 4 September 2016

Keywords:
Composite
Bolted joint
Secondary bending
Progressive damage analysis

ABSTRACT

Static tensile experiments and progressive failure simulations of single-bolt, single- and double-lap joints were carried out to comparatively investigate secondary bending effects, which present significant eccentric-loading phenomena in single-lap joints but are almost non-existent in symmetric double-lap joints. Progressive damage models of single-lap and double-lap joints were established, from which the numerical predictions were found to be in good agreement with the experimental outcomes. Experimental macro-scope failure patterns and seven numerical micro-scope failure modes obtained from the progressive damage analyses were presented for the two types of joints. The effects of secondary bending on the mechanical degradation and failure mechanism of single-lap joints were revealed. Some characterizations of secondary bending in the joints, such as a characterized parameter on the AGARD points, joint deformations and contact states, were quantitatively traced during the total progressive damage process. All these characterizations increased the understanding of the effects of secondary bending on the failure process of a single-bolt, single-lap joint.

Introduction

Composite bolted joints are widely used in aircraft structures because of their high load carrying capacity, ease of maintenance and replaceability, among other factors. However, due to the inherent complexity of composite parts, the interaction between connected components and the concentration of stress around the edge of the bolt hole, composite bolted joints exhibit extremely complicated mechanical responses, which significantly reduce the load carrying capacity of the joints and have adverse effects on the structural integrity [1,2]. Among major composite joint types, the single-lap configuration is highly representative of most composite bolted joints [2–4]. Furthermore, the aforementioned defects are particularly serious in single-lap joints because of the prominent secondary bending effects [5,6]. Secondary bending is produced by the eccentric load path with respect to the asymmetric geometry of the components, causing out-of-plane displacement and amplifying the stress concentration around the bolt hole [2,3,5]. The additional bending significantly affects the mechanical properties of single-lap joints [2,6,7]. Thus, to improve joint efficiency in aircraft structures, it is necessary to deeply understand the effects of secondary bending on the mechanical behavior of composite bolted joints [8–10].

Secondary bending was investigated in aircraft structures by Schütz and Lowak [11]. They measured the strains at 150 different structural locations and found that 86% of them presented obvious secondary bending effects. To characterize secondary bending, a parameter *SB* was defined in terms of either strains or stresses [10,12] as shown in Eq. (1):

$$SB = \frac{\varepsilon_b - \varepsilon_t}{\varepsilon_b + \varepsilon_t} = \frac{\varepsilon_{bend}}{\varepsilon_{tens}} \approx \frac{\sigma_{bend}}{\sigma_{tens}} \tag{1}$$

where the subscripts *b* and *t* indicate the bottom and top surfaces of the focused joint plates, and the subscripts *bend* and *tens* denote the quantities caused by bending and tension respectively.

Previous investigations on secondary bending have primarily used experimental methods. Strains gauges or special bending strain gauges were placed on the free surface of the investigated joint plate and in shallow grooves machined on the faying surface of the opposite member plate [6], from which the tension strains were measured and *SB* was calculated as defined in Eq. (1). Because *SB* was significantly dependent on the location of the strain gauges, especially their position in the longitudinal direction [11,12], Van der Linden [13] suggested measuring the strains at a specific point, which was named the AGARD point by the Advisory Group for Aerospace Research and Development [14] and widely used in

* Corresponding author.
E-mail address: jyzhang@cqu.edu.cn (J. Zhang).

http://dx.doi.org/10.1016/j.rinp.2016.08.021
2211-3797/

subsequent investigations on secondary bending. To avoid introducing an additional machining process and to reduce the strain sensitivity to the gauge positioning in the strain gauge method, Johan Ekh et al. [5,6] demonstrated that the curvature of a line on the focused plate surface can provide nearly identical information as *SB*. An optical full field measurement method to measure the curvature experimentally was proposed in references [5,6]. However, to obtain the curvature, the lateral displacements along the whole edge of the focused plate had to be differentiated twice over the longitudinal length, which led to computational complexity. For this reason, it can be very complicated to carry out and to assess secondary bending by quantitative analyses of curvatures along the specimen length.

In addition to the experimental investigations, some analytical models and numerical analyses of the secondary bending effects have been performed. Barrois [15] calculated the secondary bending by treating the thin plates in a single-lap joint as rigid bodies and the bolts as flexible ones. In contrast to Barrois's model, Schijve and Das et al. [3,16,17] presented a neutral line model based on the basic bending theory of elastic beams and plates neglecting the bolt effects. To simulate the characteristics of secondary bending more comprehensively, three-dimensional finite element (3D FE) analysis was increasingly used to study out-of-plane stress in composite bolted joints [18,19]. Edlund [20] developed 3D FE models to study *SB* at the AGARD points. In addition, Johan Ekh and Joakin Schön [5] also conducted detailed finite element analysis to investigate the influence of secondary bending on the strength prediction for composite joints. All these aforementioned works, however, assumed that the joints were in a linear elastic and undamaged state, which failed to reflect the actual secondary bending effects during the damage process of the joints. Thus, the knowledge of secondary bending remains deficient and the influences on mechanical behavior of typical composite joints need to be expounded more specifically and clearly.

This paper describes comparative experimental investigations on single-lap and double-lap composite bolted joints that were carried out to highlight the effects of secondary bending. In addition, a progressive damage method, which was recently developed for failure prediction of complex composite structures [21–24], was adopted here to reveal the effects of secondary bending on the failure behavior of composite bolted joints during the loading process. The experimental results agreed well with the numerical simulation, which validated the accuracy of the progressive damage model and provided confidence for the numerical analyses. The typical physical differences between the single-lap joint and double-lap joint were explained, which highlighted the secondary bending effects in the single-lap, single-bolt composite joints.

Specimens and experimental procedures

Specimens

Single-lap bolted joints and contradistinctive double-lap bolted joints were designed and fabricated according to the recommended width to hole diameter ratio ($w/d = 6$) and edge distance to hole diameter ratio ($e/d = 3$), as shown in Fig. 1. All the specimens were made of T800 carbon/epoxy composites with stacking sequences of $[45/0/-45/0/90/0/45/0/-45/0]_s$. Each composite lamina was 0.185 mm in thickness. The basic material properties were provided by the manufacturer and are listed in Table 1 [21,25].

HST12-6-5 and HST12-6-7 protruding head fasteners made of 6Al-4V titanium alloy were utilized for the single-lap and double-lap joints, respectively. They were secured by HST1078 high locking collars made of A280 high temperature alloy. The elastic modulus and Poisson ratio of the titanium alloy were 110 GPa and 0.29 and the corresponding plastic behavior are illustrated in Table 1 [21,25].

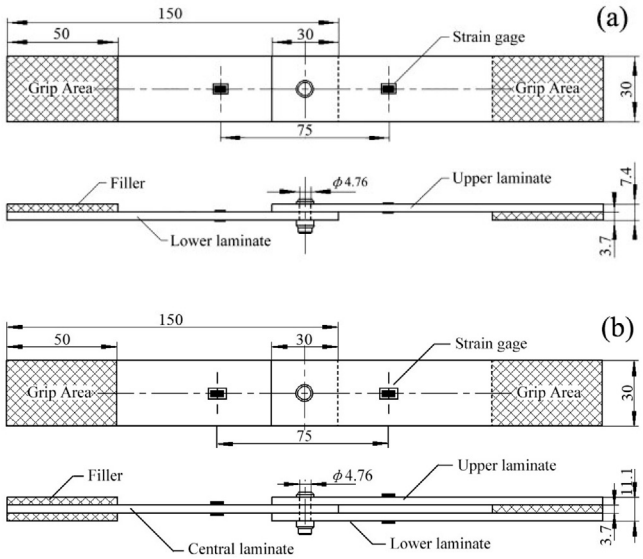

Fig. 1. Configuration and dimensions of specimens (Unit: mm) (a) specimen of single-lap joint, (b) specimen of double-lap joint.

Experimental procedures

All static tensile tests were carried out on an INSTRON-8803 testing machine with a load capability of 250 kN according to the standard ASTM D 5961 [26]. For each type of joint, five specimens were tested. To investigate the secondary bending effects in single-lap joints, a commonly used specific fixture that prevents the partial bending of the joint was not used. The tensile loads were applied to the specimens at a constant head displacement rate of 1 mm/min up to the catastrophic failure of the joints. The applied load and grip holder displacement were automatically recorded by the computer.

For each specimen, strain gauges were glued on both surfaces of the laminates, as shown in Fig. 1. During the loading process, differences between the strain gauges were calculated to evaluate the system alignment. If poor system alignment occurred, the specimen had to be reinstalled to modify the alignment. In addition, to inspect the specimen damage status, several specimens were disassembled after the experiments.

Progressive damage models for bolted joints

The progressive damage method (PDM) is acknowledged to be effective at predicting failure of composite structures due to its superiority at both forecasting the strength of complex structures and tracing the detailed failure process. To implement a progressive damage analysis, a progressive damage model is necessary. The model comprises three modules: stress analysis, failure evaluation and material property degradation.

Finite element models

To depict the stress distribution in composite bolted joints, three-dimensional finite element models of the single-lap and double-lap joints were established using ABAQUS® [27], as illustrated in Fig. 2, in which linear solid elements C3D8 were adopted. To reduce the computational cost, only half of the double-lap joint was built because of its symmetry about the mid-surface of the

Table 1
Material properties.

T800 carbon/epoxy composites				Plastic behavior of titanium alloy	
Elastic modulus/GPa		Strength/MPa		Yield stress/GPa	Plastic strain
E_{11}	195	X_T	3071	0.71	0
E_{22}	8.58	X_C	1747	0.8	0.0002
E_{33}	8.58	Y_T	88	0.85	0.0005
G_{12}	4.57	Y_C	271	0.9	0.0008
G_{13}	4.57	Z_T	88	0.97	0.002
G_{23}	2.90	Z_C	271	1.5	0.1
υ_{12}	0.33	S_{12}	143		
υ_{13}	0.33	S_{13}	143		
υ_{23}	0.48	S_{23}	143		

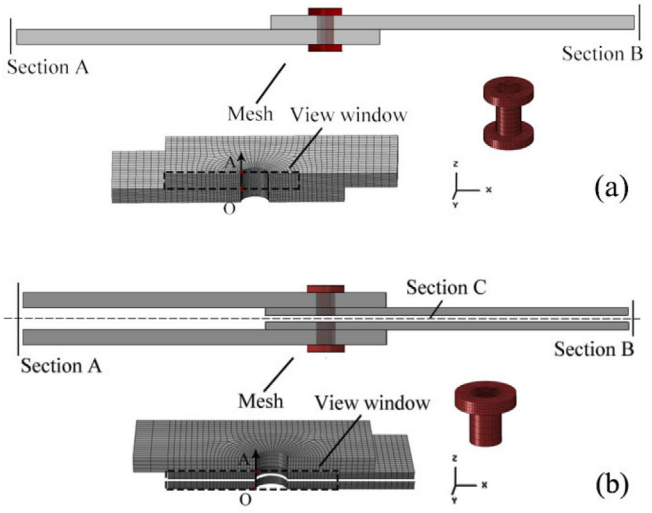

Fig. 2. Sketch of 3D finite element models (not to scale). (a) Single-lap joint model, (b) double-lap joint model.

central laminate. In addition, the bolt and nut were modeled as a unity.

Considering the stress concentration around the bolt-hole, radial fine meshes were created in the vicinity of the hole for accurate and converged numerical predictions. Relatively coarse meshes were utilized away from the hole to reduce the computational cost. Each layer was established with one element along the thickness direction in the laminate of interest, while five layers were merged in one element for the other laminates to further reduce the computational cost. A fine-meshed model of the fastener was established to accurately simulate the stress distribution around the hole edge. The nodes and elements of different parts in the models were fixed and mutually corresponded with each other.

Contact pairs were used for the interfaces between adjacent laminates as well as between the laminates and the fastener. A surface-to-surface contact method was set to obtain more accurate stress and pressure results. The friction coefficients between the laminate and metallic bolt were set at 0.3 [21], while those between the laminates were set to 0.1 [21].

Boundary conditions and loading applied to the models are indicated in Fig. 2. The nodes in section A were fixed in all three degrees of freedom and a distributed load was applied quasi-statically to section B. The nodes in section C, which is the symmetric mid-surface of the double-lap joint as illustrated in Fig. 2(b), was constrained in the z direction. A preload of 5.338 kN was applied to the bolt shank. A net-fit status was achieved by setting the diameters of the bolt and bolt hole to be equal in the model. In addition, several soft springs with stiffness factor 0.1 N/mm were attached to the bolts and plates to prevent initial rigid body motions and avoid difficulty in converging on the solution.

Failure criterion and material degradation rules

Because of the distinct and intricate failure mechanism exhibited in composite structures, diverse failure criteria and material degradation rules have been used in the literature to establish progressive damage models for various composite structures [23]. The consensus is that a suitable progressive damage model that has been verified by experiments is a prerequisite to accurate prediction of the failure of composite structures.

A Hashin-type failure criterion proposed by Shokrieh [28] and modified by Tserpes [29,30] as well as a material degradation model created by Tserpes [29,30] and modified by Zhang et al. [23] are adopted here. Their compatibility has been successfully validated by a series of experimental results [23] predicting the mechanical behavior of the same double-lap composite joints as the specimens in the current work. The failure criterion provides the capability of detecting and distinguishing seven basic microscopic failure modes in composites [23,29,30], as illustrated in Table 2. In addition, Table 2 lists the formulae of the material degradation rules [23] corresponding to each failure mode.

In Table 2, $\sigma_{ij}(i,j=1,2,3)$ are the scalar components of the stress tensor; X_t, X_c, Y_t, Y_c, Z_t and Z_c are normal strengths, in which the subscripts 't' and 'c' denote tensile and compressive status, respectively; and $S_{ij}(i,j=1,2,3)$ are shear strengths. When damage was detected, the elastic parameters and Poisson's ratios of the materials degraded according to the corresponding degradation factors represented by d_{ft}, d_{fc}, d_{mt}, d_{mc}, d_{fm}, d_{it} and d_{ic}. The subscripts 'f' and 'm' indicate fiber and matrix, respectively, and 'i' indicates interface. The following degradation factors suggested by Zhang et al. [23] were utilized in this work: $d_{ft}=0$, $d_{fc}=0.1$, $d_{mt}=0$, $d_{mc}=0.1$, $d_{mf}=0$, $d_{it}=0$, and $d_{ic}=0$, all of which were determined by a trial-and-error method based on a series of numerical tests [23].

Model validation and failure analysis

Based on the progressive damage models, the numerical stiffness, failure loads and failure modes of the single-lap joint and double-lap joint were predicted. The good agreements between the numerical and experimental results gave evidence of the effectiveness of the PDM. Typical mechanical behavior of the joints was compared to provide a deep understanding of the secondary bending effects.

Model validation

Fig. 3 shows the experimental and numerical load–displacement curves for single- and double-lap joints, numbered TSJ-1 to

Table 2
Failure criterion and Material degradation models.

Failure modes	Failure criterion	Material degradation rules
Fiber tension ($\sigma_{11} > 0$)	$\left(\frac{\sigma_{11}}{X_t}\right)^2 \geqslant 1$	$E_{11}^d = d_{ft}E_{11}$
Fiber compression ($\sigma_{11} < 0$)	$\left(\frac{\sigma_{11}}{X_c}\right)^2 \geqslant 1$	$E_{11}^d = d_{fc}E_{11}$
Matrix tension ($\sigma_{22} > 0$)	$\left(\frac{\sigma_{22}}{Y_t}\right)^2 + \left(\frac{\tau_{12}}{S_{12}}\right)^2 + \left(\frac{\tau_{23}}{S_{23}}\right)^2 \geqslant 1$	$E_{22}^d = d_{mt}E_{22}, G_{12}^d = d_{mt}G_{12}, G_{23}^d = d_{mt}G_{23}$
Matrix compression ($\sigma_{22} < 0$)	$\left(\frac{\sigma_{22}}{Y_c}\right)^2 + \left(\frac{\tau_{12}}{S_{12}}\right)^2 + \left(\frac{\tau_{23}}{S_{23}}\right)^2 \geqslant 1$	$E_{22}^d = d_{mc}E_{22}, G_{12}^d = d_{mc}G_{12}, G_{23}^d = d_{mc}G_{23}$
Fiber–matrix shear($\sigma_{11} < 0$)	$\left(\frac{\sigma_{11}}{X_c}\right)^2 + \left(\frac{\tau_{12}}{S_{12}}\right)^2 + \left(\frac{\tau_{13}}{S_{13}}\right)^2 \geqslant 1$	$G_{12}^d = d_{fm}G_{12}, v_{12}^d = d_{fm}v_{12}$
Interface tension ($\sigma_{33} > 0$)	$\left(\frac{\sigma_{33}}{Z_t}\right)^2 + \left(\frac{\tau_{13}}{S_{13}}\right)^2 + \left(\frac{\tau_{23}}{S_{23}}\right)^2 \geqslant 1$	$E_{33}^d = d_{it}E_{33}, G_{23}^d = G_{13}^d = v_{23}^d = v_{13}^d = 0$
Interface compression ($\sigma_{33} < 0$)	$\left(\frac{\sigma_{33}}{Z_c}\right)^2 + \left(\frac{\tau_{13}}{S_{13}}\right)^2 + \left(\frac{\tau_{23}}{S_{23}}\right)^2 \geqslant 1$	$E_{33}^d = d_{ic}E_{33}, G_{23}^d = G_{13}^d = v_{23}^d = v_{13}^d = 0$

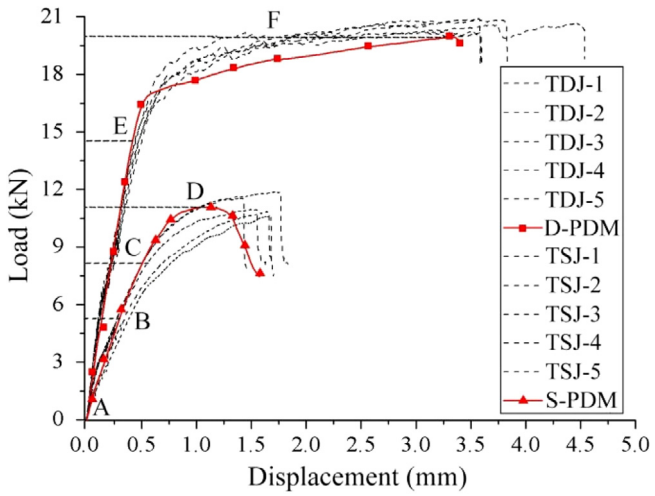

Fig. 3. Numerical and experimental load–displacement curves for the single-lap and double-lap joints.

5 and S-PDM, TDJ-1 to 5 and D-PDM, respectively. Points A through F denote typical states. For both types of joints, the numerical curves are in good agreement with the experimental curves, which demonstrates that the finite element model and progressive damage model can simulate the initial stiffness and subsequent stiffness degradation of the joints accurately. Table 3 further lists the predicted and experimental failure loads of the single-lap and double-lap joints. For both types of joints, the variation coefficients of the experimental data are no more than 5%, which indicates that the scatter of the experimental data is small. In addition, the numerical prediction errors for the failure loads of the joints are less than 5%, which indicates that the progressive damage model can forecast the failure loads accurately. This progressive damage model can reproduce the load–displacement curves and accurately predict the failure loads, which gives evidence of the effectiveness of the model.

From Fig. 3 and Table 3, the difference between single-lap and double-lap bolted joints can be observed, and the secondary bending effects can be depicted. In the single-lap joints, the curves started to deflect from linear behavior at the initial failure load (approximately 8 kN) and then entered a significant softening phase. Quickly, the single-lap joints arrived at their peak loads and lost their load-bearing capability. The final failure displacement of the single-lap joints was approximately 1.5–2 mm shorter than that of the double-lap joints, which ranged from 3.5 to 4.5 mm. In addition, the average failure load of the single-lap joints was approximately 11 kN, which was close to half that of double-lap joints. In the double-lap joints, the curves exhibited steady a linear growth until the initial failure occurred (approximately 15 kN). The slopes decreased sharply due to severe composite degradation. The advents of several small jumps and waves indicated that the bearing damage kept on propagating in the joints. However, these curves soon showed another approximately linear stage, which indicated that even though the joints were suffering substantial damage, their load-bearing capability continued to strengthen.

Failure analysis

Fig. 4 gives the experimental failure patterns of the upper laminate of a single-lap joint and the central laminate of a double-lap joint, respectively. Both joints experienced bearing damage ahead of the bolt hole.

For the single-lap joint, secondary bending effects were observed in the slanted hole wall and the larger deformation of the hole on top of the laminate than on the bottom. Minor bearing damage with crimping occurred ahead of the hole, which slightly expanded the circle of the hole. In contrast to the single-lap joint, the bolt in the double-lap joint horizontally pushed the laminates ahead of the hole to form a runway-shaped orifice, which resulted

Table 3
Strength comparison between experiments and PDMs simulation.

Specimen No.	Experimental failure load (kN)	Average failure load (kN)	Coefficient of variation (%)	Predicted failure load (kN)	Error (%)
TSJ-1	10.70	11.26	4.23	11.09	−1.51
TSJ-2	12.00				
TSJ-3	11.10				
TSJ-4	11.60				
TSJ-5	10.90				
TDJ-1	21.18	20.83	1.53	19.93	−4.32
TDJ-2	20.88				
TDJ-3	20.78				
TDJ-4	21.06				
TDJ-5	20.26				

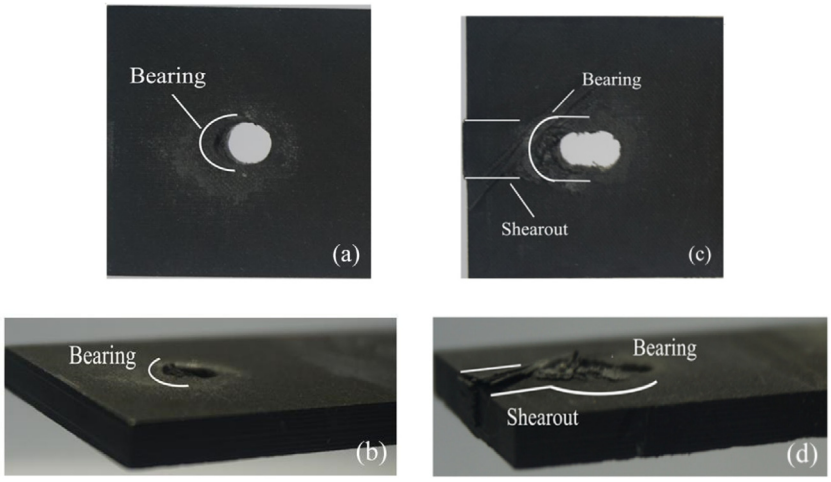

Fig. 4. Experimental failure patterns of laminate in the joints. (a) Top view of the upper laminate in the single-lap joint. (b) Axial view of the upper laminate in the single-lap joint. (c) Top view of the central laminate in the double-lap joint. (d) Axial view of the central laminate in the double-lap joint.

in severe bearing damage and shear damage exhibited on the surface of the plate of interest. Clearly, a slight degree of damage in single-lap joints led to an obvious reduction of the load carrying capability, while the double-lap joints could withstand more severe damage.

The failure contours of the upper plate of the single-lap joint and the central plate of the double-lap joint were extracted after the final failure examination. Fig. 5 illustrates failure contours in the two types of joints, including the comprehensive failure contours and those corresponding to seven micro-scale failure modes. The view windows of the profiles in Fig. 5 cover the area denoted by dashed rectangles in Fig. 2(a) and (b). For contrast, the failure contours of the whole central plate in the double-lap joint are plotted according to the structural symmetry. Failure zones are marked in gray to clearly identify the failure status in the two types of joints.

The comprehensive damage zones shown in Fig. 5(a) and (i) are mainly induced by inter-laminar compression failure (Fig. 5 (h) and (p)) and fiber–matrix shear failure (Fig. 5(f) and (n)). In addition, fiber (Fig. 5(c) and (k)) and matrix compression (Fig. 5 (e) and (m)) in the transverse direction also give rise to conspicuous damage areas in the joints. There is only minimal damage around the bolt hole due to fiber, matrix, or interlaminar tension failure, as depicted in Fig. 5.

From Fig. 5(a)–(h), it can be observed that the damage zone in the single-lap joint was anti-symmetric and approximately triangular in shape, which was caused by the bolt inclination and the laminate warp due to the secondary bending effects. The damage in the lower-left corner around the hole and that on the upper-right surface of the laminate were especially serious. In contrast, in Fig. 5(i)–(p), the damage zones in the double-lap joint were relatively uniform along the hole edge. They were much larger than those in the single-lap joints and extended to the end of the laminate. This pattern of damage suggests that the double-lap joint achieved a higher efficiency of material utilization than the single-lap joint, which is in agreement with the catastrophic shear-out and bearing damage presented in Fig. 4.

Quantitative analysis of secondary bending effects in progressively damaged joints

Secondary bending can be described by a bending moment that results from the eccentric load applied to the joints. The bending moment is balanced by the reaction of the surrounding structures in the joint during the loading procedure, which leads to some non-linear deformations including warping of the laminates, slanting of the fasteners and deformation of the fastener hole, among other deformations. Here, some typical physical factors, namely, the secondary bending (*SB*) at the AGARD point, the contact areas and the slant of the fastener were investigated to characterize the secondary bending effects.

Secondary bending

From the numerical results, the secondary bending (*SB*) was calculated from the strains located at the AGARD points [14] and plotted in Fig. 6, in which different load levels corresponding to Points A to F in Fig. 3 are marked. Because the initial load applied to the joints was affected primarily by the static friction force, the strains produced by the bending and tension of the plate were both very small, which led to a singular *SB* value.

For the single-lap joint, the value of *SB* increased quickly as the applied load increased and then rose linearly at a slow rate up to the final failure range between 1.6 and 1.9 (from Point B to D). During this period, the joint experienced gradual damage propagation and stiffness reduction. After that, the joint arrived at its peak load and quickly lost its load carrying capability with a sudden fluctuation of *SB* to over 2.0 (Point D).

In contrast, the secondary bending in double-lap joints was very small (in the range of 0.2–0.4) before the initial damage occurred and much less than that in single-lap joints. Compared with single-lap joint, the value of *SB* slightly decreased as the load increased. When damage occurred in the joint (Point E), resulting in a reduction of the joint stiffness, the secondary bending rapidly increased. Eventually, *SB* in the double-lap joint reached approximately 0.8, which corresponds to the final failure load marked by Point F.

Deformation and contact states

From the progressive damage analysis of the bolted joints, the deformation of the joint can be captured throughout the loading process, as shown in Fig. 7. A tilt angle was defined between a line normal to the composite plate and the line connecting the geometrical center of the bolt head and the nut to measure the local deformation of the joint. Because of the geometrical symmetry, the tilt angle in the double-lap joint was identically equal to zero. The tilt angle was extracted from the numerical results and the curve of

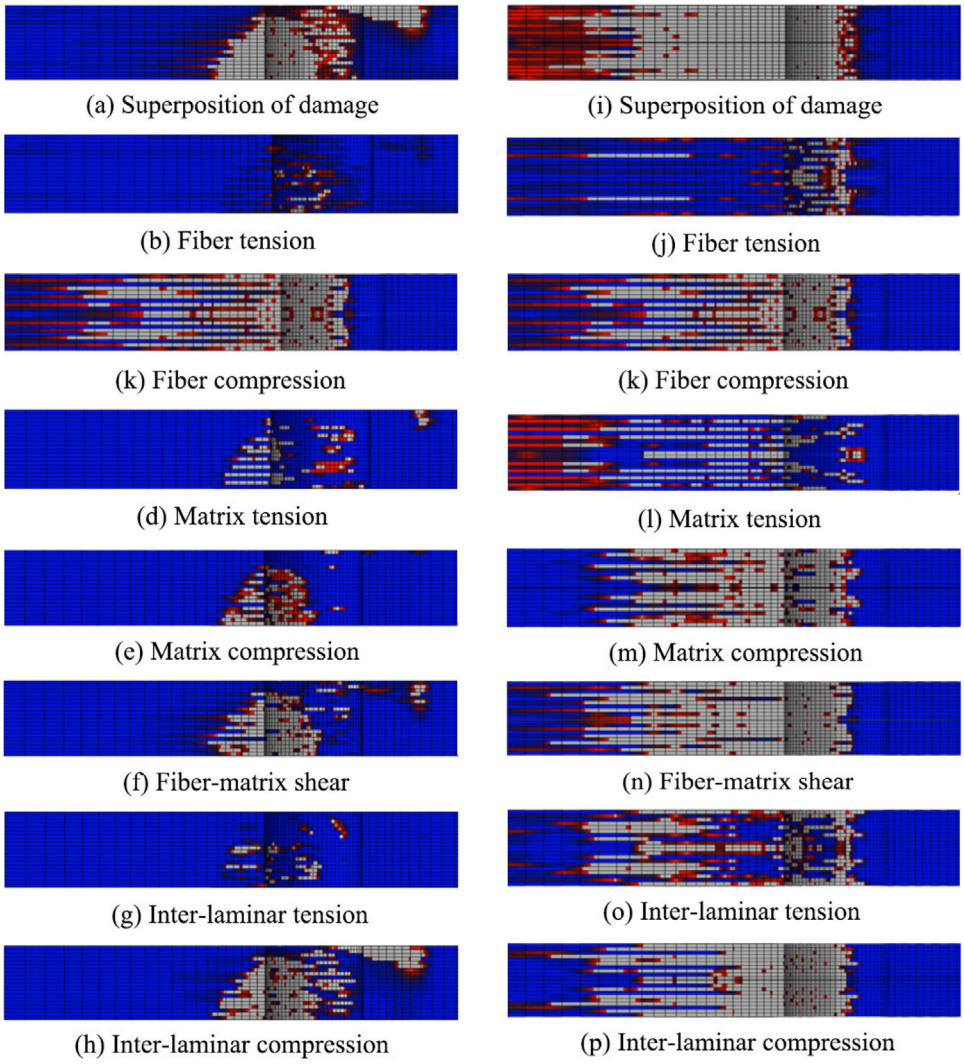

Fig. 5. Profile charts of failure contours in the single-lap and double-lap joints. (a)–(h) Single-lap joint (i)–(p) Double-lap joint.

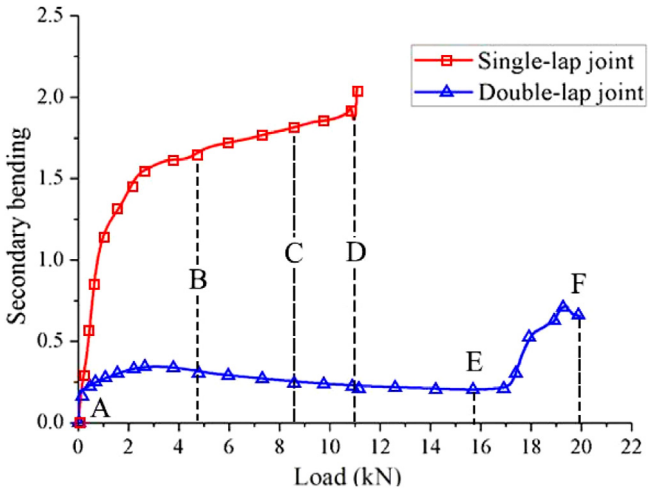

Fig. 6. Changes of secondary bending during the damage propagation process.

the tilt angle versus the applied load is plotted in Fig. 7(a). The tilt angle in the single-lap joint grew continuously with the applied load. At first, it increased linearly from Point A to Point C. With increasing applied load, the slope of tilt angle vs. load gradually increased as the damage accumulated in the joint reduced the joint stiffness and made the bolt deflection easier. When the damage had accumulated to some extent, the tilt angle rapidly jumped from 6 degrees to 8 degrees, corresponding to the catastrophic final failure (Point D) in the single-lap joint.

The local deformation and damage zones of both joints under typical load states are also extracted and concisely illustrated in Fig. 7(a). For the single-lap joint, the secondary bending led to the tilt of the fastener and the warp of the laminates. It exacerbated the uneven deformation and asymmetric stress distribution around the bolt hole, which brought about material damage in the joint. Subsequently, the composite materials around the hole wall suffered from the more intense stress concentration and gradually failed. As the applied load increased, the bolt in the single-lap joint tilted more severely and the triangular damage zone developed rapidly in the laminate. As a result, the contact area between the fastener and the hole wall became much smaller, and finally the joint lost its load-bearing capacity. With respect to the double-lap joint, however, the deformation distribution of the center laminate (i.e., the laminate of interest) was relatively uniform. It could be deduced that the stress was evenly distributed along the thickness direction, which resulted in a consistent compression of the material ahead of the hole. Thus, the double-lap joint was still

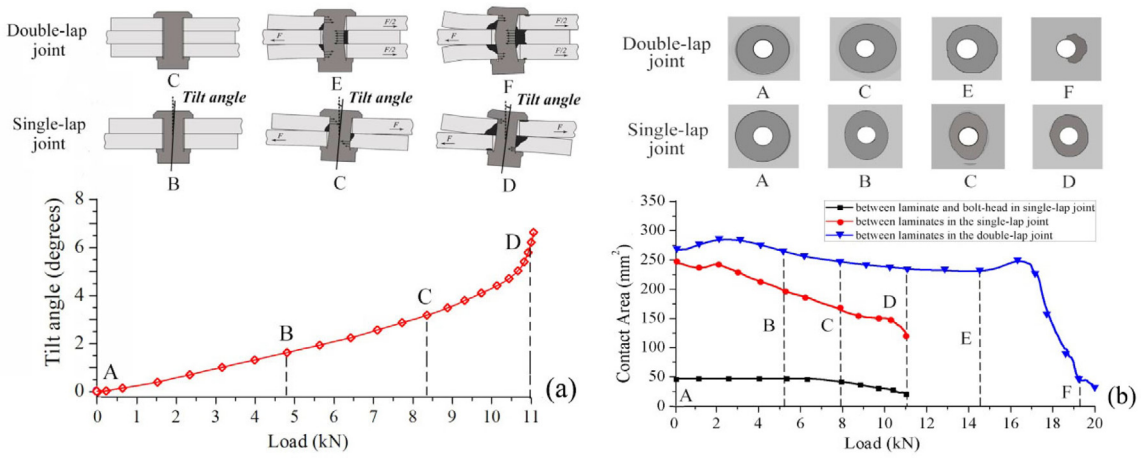

Fig. 7. Deformation and contact states in single-lap and double-lap joints. (a) Tilt angle and deformation sketch, (b) contact area on the faying surface.

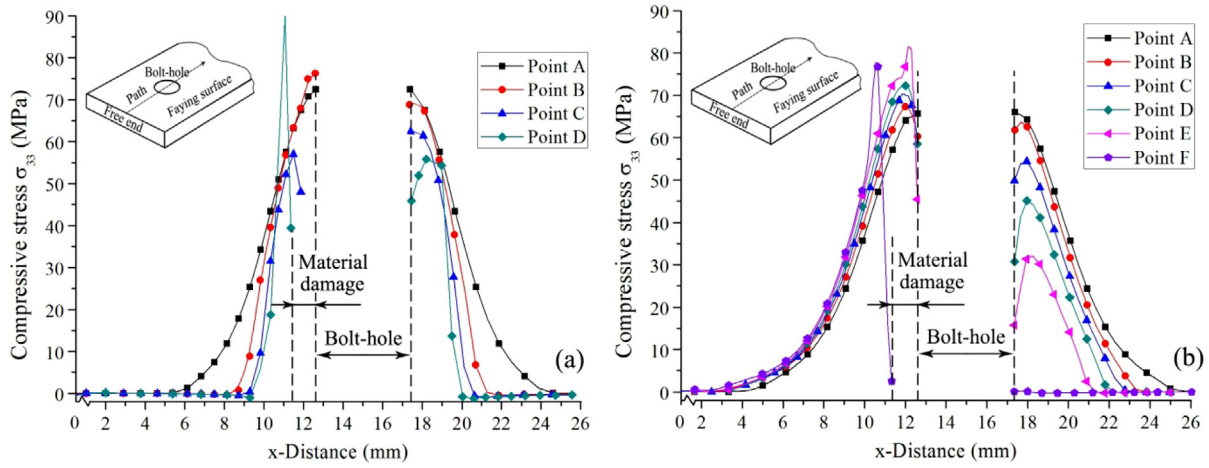

Fig. 8. Compressive stress variation along the path in the axial direction. (a) Stress distributions in the single-lap joint (b) stress distributions in the double-lap joint.

effective, although all the surface materials along the hole wall were destroyed.

The contact areas, which changed during the loading process, also reflected the secondary bending effects in the joints. Fig. 7(b) shows the contact area vs. load curves, which shows the contact between the laminates of the single-lap joint, between the laminate and the bolt-head of the single-lap joint, and between the central laminate and the upper or bottom laminate of the double-lap joint. In the single-lap joint, the bolt head maintained contact with the laminate until the onset of damage. With damage propagation, the bolt head gradually separated from the laminates gradually. However, slight changes followed by obvious drops were detected for the contact areas between the laminates in both single- and double-lap joints. The contact areas decreased much more quickly in the single-lap joint, which meant that the laminates tended to separate from each other due to severe bending deformation. In addition, the contact area between the two laminates in the single-lap joint and that between the upper laminate and central laminate in the double-lap joint are illustrated in dark gray.

The contact area between two laminates is correlated with contact force, as shown in Fig. 8. The stresses on the faying surface in the axial direction were extracted under several load levels (corresponding to Points A–F) in both types of joints. The stress levels were similar for both types of joints because the initial contact states were primarily determined by the preload force. Since the preload was applied on the fastener shank, the stress increased gradually in the direction of the bolt hole, and the largest compressive stress appeared near the hole edge. At the same time, the contact area near the free end was similar to that away from the free end.

During the loading process, the contact area decreased and the contact stress away from the bolt head quickly decreased in the single-lap joint. As shown in the single-lap joint in Fig. 8(a), the diameter of the contact area between laminates decreased from 3.7 to 2.0 times the bolt hole diameter as the damage propagate, which could be explained by the laminate warp reducing the contact areas in the joint. In the double-lap joint, the stress level near the free end increased slightly and the diameter of the contact area remained approximately 5.0 times the bolt hole diameter in Fig. 8 (b). On the other side, the stress level away from the free end gradually decreased with the applied load. The diameter of the contact area ranged from 3.4 to 2.7 times the bolt hole diameter. The change depicted in Fig. 8 is consistent with the diagrams of local deformation and the contact states in Fig. 7. From these results, it can be concluded that the higher stress level and decreased contact area caused by secondary bending further accelerated the material damage in the single-bolt, single-lap joint.

Conclusion

In this work, a combination of experimental and numerical methods was utilized to investigate the secondary bending effects on the mechanical behavior of a single-bolt, single-lap joint by comparison with a double-lap joint. Progressive damage analyses of both types of joints were implemented to investigate their different load-bearing mechanism and the effects of secondary bending during the progress toward total failure. Good agreements was achieved between the experimental and numerical results, which proved the effectiveness of the progressive damage models. The results showed that the single-bolt, single-lap joint had a nonlinearity onset strength that was lower by half than that of the double-lap joint. The average final failure load of the single-lap joint was 85% lower than that of the double-lap joint.

Experimental macro-scope failure patterns of the two types of joints and seven numerical micro-scope failure modes obtained from the progressive damage analyses were studied. Bearing damage was dominant in the single-lap joint, while both shear-out damage and bearing damage were very severe in the double-lap joint. According to the seven micro-scope failure contours, the damage zones in the single-lap joint were not symmetric and were approximately triangular in shape, which was caused by the inclination of the bolt and the warp of the laminate due to secondary bending effects. However, the damage zones in the double-lap joint were relatively uniform along the hole wall, which resulted in a higher load-bearing capability in the double-lap joints.

The *SB* at the AGARD point changed linearly from 1.6 to 2.0 in the single-lap joint while remaining approximately 0.3 in the double-lap joint, after which it suddenly rose for both types of joints due to the occurrence of the final failure. The tilt angle in the single-lap joint, as a typical characteristic of secondary bending, was found to increase with the load and finally reached 7.6 degrees as the damage extended. Moreover, as a result of the local deformation caused by the secondary bending, the contact area decreased rapidly and sped up the material damage in the single-bolt, single-lap joint.

Acknowledgements

This research is supported by the National Science Foundation of China (11572058 and 11372020) and the China Postdoctoral Science Foundation (2015M580956).

References

[1] McCarthy CT, Gray PJ. An analytical model for the prediction of load distribution in highly torqued multi-bolt composite joint. Compos Struct 2011;93:287–98.
[2] McCarthy MA, McCarthy CT, Lawlor VP, Stanley WF. Three-dimensional finite element analysis of single-lap composite bolted joint part 1 – model development and validation. Compos Struct 2005;71:140–58.
[3] Schijve J, Campoli G, Monaco A. Fatigue of structures and secondary bending in structural elements. Int J Fatigue 2009;31:11–23.
[4] DODSSP, Polymer matrix composites, MIL-HDBK-17, DODSSP, Naval Publications and Forms Center, Standardization Documents Order Desk. Building 4D, 700 Robbins Ave. Philadelphia, PA [1911-5094].
[5] Ekh Johan, Schon Joakim. Effects of secondary bending on strength prediction of composite, single shear lap joints. Compos Sci Technol 2005;65:953–65.
[6] Ekh Johan, Schon Joakim, Gunnar Melin L. Secondary bending in multi fastener, composite-to-aluminum single shear lap joints. Compos B 2005;36:195–208.
[7] Skorupa M, Korbel A, Skorupa A, Machniewicz T. Observations and analyses of secondary bending for riveted lap joints. Int J Fatigue 2015;72:1–10.
[8] Olmedo A, Santiuste C, Barbero E. An analytical model for the secondary bending prediction in single-lap composite bolted-joints. Compos Struct 2014;111:354–61.
[9] Ireman T. Three-dimensional stress analysis of bolted single-lap composite joints. Compos Struct 1998;43(3):195–216.
[10] Egan B, McCarthy CT, McCarthy MA, Frizzell RF. Stress analysis of single-bolt, single-lap, countersunk composite joints with variable bolt-hole clearance. Compos Struct 2012;94(3):1038–51.
[11] Schütz D, Lowak H. The effects of secondary bending on the fatigue strength of joints, report FB-113. Darmstadt: Laboratorium fur Betriebsfestigket; 1974.
[12] Muller RPG. An experimental and analytical investigation on the fatigue behavior of fuselage riveted lap joints. The significance of the rivet squeeze force, and a comparison of 2024-T3 and glare 3 [Ph.D. thesis]. The Netherlands: Delft University of Technology; 1995.
[13] Van der Linden HH. Determination of secondary bending and load transfer. NLR Memorandum SB-81-083U.
[14] Van der Linden HH. Fatigue rated fastener system—an AGARD coordinated testing program. Technical Report AGARD No. 721, National Aerospace Laboratory, NLR, Amsterdam; 1985.
[15] Barrois W. Stress and displacements due to load transfer by fasteners in structural assemblies. Eng Fract Mech 1978;10:115–76.
[16] Schijve J. Some elementary calculations on secondary bending in simple lap joints, Report NLR TR 72036. Amsterdam: NLR; 1972.
[17] Das GK, Miller M, Sovar T. Durability assessment of fuselage single shear lap joint with pads. In: Rouchon J, editor. Design for durability in the digital age. proceedings of the 21th ICAF symposium, 27–29 June 2001. France: Cepadues Edition; 2001.
[18] Ireman T. Three-dimensional stress analysis of bolted single-lap composite joints. Compos Struct 1998;43:195–216.
[19] Ireman T, Ranvik T, Eriksson I. On damage development in mechanically fastened composite laminates. Compos Struct 2000;49:151–71.
[20] Edlund A. Ickelinjar FE-analys av sekundärböjningen i kompositskruvforband [Master's thesis]. Linkopings Tekniska Hogskola; 1985. LiTH-IKP-Ex-531, [In Swedish].
[21] Qin TL, Zhao LB, Zhang JY. Fastener effects on mechanical behaviors of double-lap composite joints. Compos Struct 2013;100:413–23.
[22] McCarthy CT, McCarthy MA. Three-dimensional finite element analysis of single-bolt, single-lap composite bolted joints: Part II – effects of bolt-hole clearance. Compos Struct 2005;71:159–75.
[23] Zhang JY, Liu FR, Zhao LB, Chen YL, Fei BJ. A progressive damage analysis based characteristic length method for multi-bolt composite joints. Compos Struct 2014;108:915–23.
[24] Zhao LB, Qin TL, Shenoi RA, Zhang JY, Liang XZ, Huang H. Strength prediction of composite p joint under tensile load. J Compos Mater 2010;44(23):2759–78.
[25] China aeronautical materials hand book, V25–62, 2001. [In Chinese].
[26] ASTM standard D 5961/D 5961M–96, Standard Test Method for Bearing Response of Polymer Matrix Composite Laminates; 1996.
[27] Abaqus-Inc. Abaqus user manual, Version 6.10; 2010.
[28] Shokrieh M, Lessard L, Poon C. Three dimensional progressive failure analysis of pin/bolt loaded composite laminates. In: The 83rd meeting of the AGARD SMP on bolted joints in polymeric composites. Italy; 1996.
[29] Tserpes KI, Papanikos P, Kermanidis T. A three-dimensional progressive damage model for bolted joints in composite laminates subjected to tensile loading. Fatigue Fract Eng Mater Struct 2001;24:663–75.
[30] Tserpes KI, Labeas G, Papanikos P, Kermanidis TH. Strength prediction of bolted joints in graphite/epoxy composite laminates. Compos Part B 2002;33:521–9.